

N.A. Shydlovska, S.M. Zakharchenko, M.F. Zakharchenko, M.A. Kulida, S.A. Zakusilo

Spectral and optic-metric methods of monitoring parameters of plasma channels caused by discharge currents between metals granules in working liquids

Introduction. Spark-erosion processing of metals and alloys granules in working liquids is the basis of a several technological processes. Efficiency of energy use in them and parameters of the resulting product largely depend on the accuracy of stabilization and regulation of pulse power in each plasma channel between the granules. To achieve this, until now only the voltage and current of the discharge pulses in the entire layer of granules have been controlled. **Problem.** The measurement methods, which are used, are not effective enough for monitoring the parameters of individual plasma channels and predicting the size distribution of eroded metals particles at the stage of their formation. The **aim** of the work is to develop a method for determining the volumes of components of plasma channels in layers of metals granules during their spark-erosion treatment to predict the size distribution of eroded metal particles at the stage of their formation, as well as to simplify the method of spectrometric analysis of the elemental composition of substances surrounding plasma channels for the operational prediction of the chemical composition of resulting products. **Methodology.** A series of experiments were carried out on spark-erosion processing of Al and Ag granules layers in distilled water. Using a digital camera, images of the plasma channels in them were obtained. Based on the theory of pulsed electrical breakdown of liquid dielectrics, an analysis of the components of plasma channels was carried out. Using the specialized ToupView program, the volumes of equivalent ellipsoids of rotation were determined, approximating the halos of colored radiation likely arising from streamers, as well as the spark cores of plasma channels emitting white light. The shades of the resulting radiation were studied for several metals and working liquids. The obtained data were compared with the known results of spectrometric studies for the same elements excited by similar mechanisms. **Results.** The theory of discharge-pulse systems for spark-erosion processing of granular conductive media has been developed in the direction of new methods for monitoring the parameters of discharge pulses and predicting the chemical composition and size distribution parameters of eroded metal particles at the stage of their production. An optic-metric method has been developed for determining the volumes of halos and cores of plasma channels. A simplified spectral method for determining the chemical composition of erosion particles based on the shade of the resulting radiation was proposed. **Originality.** The developed new optic-metric method makes it possible to obtain information about almost every plasma channel, which refines predictions of the size distribution of erosion particles. To implement the method, general-purpose hardware and specialized software that is freely available are used. The developed method of simplified spectral analysis of excited atoms makes it possible to make preliminary predictions of the chemical composition of the obtained erosion particles already at the stage of their formation without the use of expensive specialized equipment. **Practical significance.** The ratio of the volumes of halos and cores of plasma channels between Al and Ag granules in distilled water was measured. An analysis of the emission spectra of plasma channel halos between Al, Ag and Cu granules in distilled water, Fe in ethyl alcohol, Ni-Mn-Ga and Ti-Zr-Ni alloys in liquid nitrogen, and Ti-Zr-Ni in liquid argon was carried out. Based on spectrometry data, the resulting shades of these radiations were substantiated and their description in the RGB system is given. References 56, table 1, figures 4.

Key words: discharge current, plasma channels, metal granules, optical emission spectrum.

Обґрунтовано актуальність та доцільність розроблення та застосування оптичних методів контролю параметрів плазмових каналів у шарах металевих гранул під час їх іскро- та плазмоерозійного оброблення з метою підвищення точності керування процесами і якості продукції, яка отримується. Розроблено оптикометричний метод визначення відношення об'ємів кольорових ореолів, імовірно спричинених стримерами, та іскрових ядер плазмових каналів між гранулами металів у робочій рідині, який не потребує спеціалізованого спектрометричного обладнання, а базується на використанні апаратних засобів загального призначення та спеціалізованого програмного забезпечення, яке є у вільному доступі. Даним методом проведено аналіз відношення об'ємів кольорових ореолів та іскрових ядер плазмових каналів між гранулами Al та Ag у дистильованій воді, що дало додаткову інформацію для прогнозів співвідношення нано- та мікророзмірних фракцій ерозійних частинок металів на етапі їх формування. Проведено аналіз спектрів випромінювання кольорових ореолів плазмових каналів у дистильованій воді між гранулами Al, Ag, Fe та Cu, а також Ni-Mn-Ga та Ti-Zr-Ni у рідкому азоті і Ti-Zr-Ni у рідкому аргоні. Обґрунтовано і узагальнено відтінки результуючого випромінювання у цих випадках та наведено їх опис за RGB-кодами. Обґрунтовано можливість спрощення спектрометричного методу аналізу плазми та оточуючої її парогазової фази у шарах металевих гранул за аналізом відтінку результуючого випромінювання, який базується на отриманих раніше спектрометричних даних. Бібл. 56, табл. 1, рис. 4.

Ключові слова: розрядний струм, плазмові канали, металеві гранули, оптичний спектр випромінювання.

The current state of research, definition and relevance of the problem. Spark and plasma erosion processing of layers of metal granules (LMGs) in working liquids with relatively low specific electrical conductivity is the basis of four groups of technological processes. The first one is the production of microdispersed powders of metals and alloys with special properties: refractory and heat-resistant, with magnetic [1] and temperature [2] shape memory, with amorphous [3] and amorphous-crystalline structure [4], with a giant magnetoresistive effect [5], soft-magnetic [6], hydrogen-absorbing [7],

solid [8], corrosion-resistant [9], etc. [10, 11]. The second one is spark plasma or electric discharge sintering under pressure of micro-sized powders of metals and alloys in composites, ceramics and other heterogeneous media [12]. The third one is the production of coagulant-forming hydroxides of metals (Al and Fe) for purification, including for the needs of thermal power energy industry [13] and disinfection [14] of natural waters and industrial waste water. The fourth one is the production of sedimentation-resistant nanodisperse hydrosols of biologically active metals (Ag, Cu, Zn, Fe, Mg, Mn, Mo,

Co) [15, 16] for use in plant breeding [17] and animal breeding [18].

The process is as follows. As a result of the supply from the generator of discharge pulses of electrical energy to the LMG immersed in the working liquid, a current begins to flow in it. The conditions in the contacts between the granules change rapidly and to some extent stochastically even during one discharge pulse, which leads to the branching and migration of current flow channels in the LMG, the direction of which is determined by the smallest electrical resistance of the circuit, and not by the shortest distance between the electrodes. In LMG, as a rule, there are simultaneously several parallel paths of current flow from one electrode to another.

Under the conditions of low values of the amplitude of the discharge voltage pulses (up to ≈ 40 V), plasma channels between the surfaces of the granules do not appear. In this case, the current between the granules flows through the working liquid, which is characterized by low ionic conductivity, or through ohmic contacts with low resistance between the granules, which happens less often. With a further increase in the amplitude of the voltage pulses between some pairs of granules, first streamer, and later spark channels, begin to form.

A further increase in the voltage of the discharge pulses leads to an increase in the number of both serially and parallel connected plasma channels in the LMG. When the average amplitude of voltage pulses is greater than ≈ 36 V for each consecutively connected contact between granules, plasma channels appear in the direction from electrode to electrode throughout the LMG. In operation modes, the amplitude of voltage pulses usually does not exceed 20 V on average for each contact connected in series. The duration of pulses is from units to tens of microseconds, and the average power during this time is from tens to hundreds of kilowatts.

Depending on a number of conditions [19], part of the streamer channels evolves in the spark, and the rest stops at the pre-spark stages of the streamer or leader [20]. One of the significant differences between streamer-leader channels and spark channels is the orders of magnitude lower energy released in them [20, 21]. As a result, eroded metal particles formed due to the action of streamers or leaders most often have sizes from tens to hundreds of nanometers [16], and those formed as a result of the action of sparks – from units to tens of micrometers [10]. Forced limitation of the evolution of most plasma channels by pre-spark stages with the help of special measures [15, 16, 22] made it possible to create new ones – plasma erosion, based on earlier spark-erosion technologies, in particular, the third and fourth groups. Their energy and material efficiency largely depend on the ratio of streamer-leader and spark channels in LMG.

Until now, in most cases, this ratio was controlled indirectly by measuring the amplitude and duration of the discharge current pulses throughout the LMG [22], which is the sum of all branches of the discharge currents in the gap between the electrodes. But this method does not take into account changes during the discharge pulse of the

number of plasma channels in the LMG and the plane of their cross sections, as a result of which it does not provide comprehensive information about the current density in them. Therefore, it is insufficient to control the above ratio. In addition, visual observation of plasma channels by the process operator without the use of special devices is used, but it is subjective and not sufficiently accurate. Therefore, an urgent and important task is the search for objective and sufficiently accurate methods of controlling the ratio of streamer-leader and spark channels in LMG.

The goal of the article is to develop a method of objective optical determination of the volumes of streamer-leader and spark components of plasma channels in LMG during their spark and plasma erosion processing, the ratio of these volumes, as well as to simplify the method of spectrometric research of the elemental composition of the surrounding plasma channel of a steam-gas phase and working liquid and impurities in it for some metals and working liquids by analyzing the resulting shade of radiation. These methods are new in operational control of electrotechnological processes of spark- and plasma-erosion processing of LMG and allow more accurate prediction of the granulometric and chemical composition of erosion particles even at the stage of their production. The development of laws for regulating the distribution of erosion particles by size using the results of the analysis of the specified volumes of plasma channel elements and their ratio as information parameters, and the parameters of discharge pulses as controls, and the creation of automatic regulation systems with their involvement will allow to improve the accuracy of property control in the future erosion particles.

Methodology of experiments, equipment, modes and materials. The objects of research were plasma channels in layers of aluminum and silver granules immersed in distilled water. The experiments were carried out on a laboratory installation for spark and plasma erosion processing of LMG, the functional diagram of which is presented in Fig. 1. The installation included: a thyristor discharge pulse generator (marked DPG). A generator control unit (CU), a discharge chamber (DC) with a LMG immersed in the working liquid (marked DCham), a vibration bench (VB), on which it was located, a C8-17 memory oscilloscope (Osc), a voltage divider 1:10 (Voltage probe, VProbe), a high-frequency measuring current transformer (Current probe, CProbe), a web camera (WCam), connected to a personal computer (PC).

The generator was powered by a single-phase network with voltage of 220 V and frequency of 50 Hz (220V). The network voltage was rectified, regulated and stabilized by a controlled thyristor-diode rectifier (CR) and filtered from the alternating component by capacitor C1.

The operating capacitor C was charged to almost twice the voltage of the filter capacitor C1 at the command of the generator control unit through a charging circuit with Q factor greater than 20, which included

thyristor VS1 and choke L1. The charge voltage of the operating capacitor C, the capacity of which in our experiments was 100 μF , was adjusted by adjusting the voltage on the filter capacitor C1. After the end of the discharge process and closing thyristor VS1 in a natural way, according to the next command of the control unit, discharge thyristor VS2 was opened. The voltage of the operating capacitor through VS2 and the connecting cable with inductance L, which in our experiments was $\approx 2 \mu\text{H}$, was applied to the discharge chamber, where it caused the appearance of plasma channels in the LMG. After the end of the discharge, according to the commands of the control unit, the charge of the next pulse-following cycle began.

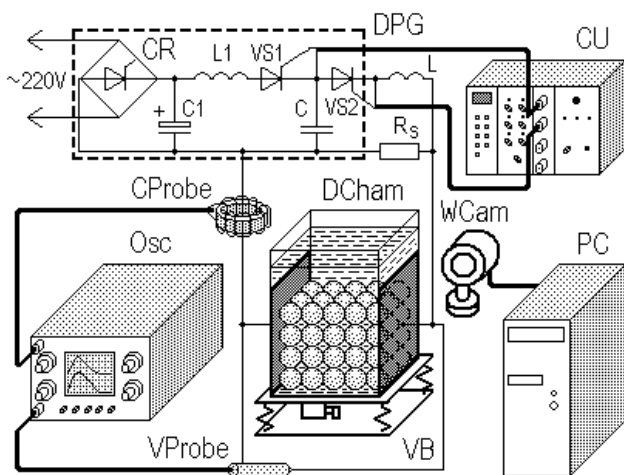


Fig. 1. Functional diagram of the laboratory installation

The discharge current was almost always aperiodic. Oscillating discharges could occur due to the stochastic decrease in the equivalent electrical resistance of the LMG, but they were almost never observed in our experiments. More dangerous for such thyristor generators (Fig. 1) is a stochastic increase in the resistance of the LMG, as a result of which a current flows through it, which slightly exceeds the holding current of the discharge thyristor VS2. If the duration of the discharge process under such conditions exceeds the duration of the pause between the discharge and charge pulses, a situation may arise when the discharge thyristor VS2 has not yet closed, and the charge thyristor VS1 has already opened. That is, a situation may arise when all thyristors will be open for a long time and not only the energy of capacitor C will enter the load, but also almost all the energy of capacitor C1, and in the worst case, even the energy of the power supply network, the current of which will be limited only by the parameters of the choke L1 and the load.

Such modes can cause not only an overload by current of the thyristors of the generator, but also the fusion of metal granules in the DC with each other, which will make their further processing impossible. To prevent these modes, a resistive shunt R_s is connected in parallel with the load in Fig. 1. In our experiments, its resistance was 3 Ω , which ensured an almost complete discharge of the operating capacitor C and the closing of the thyristor VS2 in a natural way before the arrival of the next

charging pulse, despite the stochastic increase in the resistance of the LMG. The pulse repetition rate in these experiments was 50 Hz.

In more detail, the operation of laboratory equipment for spark and plasma erosion processing of LMG, on which experiments were carried out with aluminum granules, is described in [23], and with silver granules in [16]. A7E aluminum granules were quasi-spherical in shape with diameter of $\approx 4 \text{ mm}$, and their surface had previously undergone spark electroerosion treatment. The distance between the vertical aluminum electrodes of the AD0 brand in the discharge chamber No. 1 was 52 mm. The height of the LMG is 30 mm, the width is 22 mm. The flow of water in this case was directed from the bottom up and was $\approx 12 \text{ ml/s}$, which ensured the stability of the process and removed eroded particles from the active zone of the DC. Forced vibration activation [15] with frequency of $\approx 90 \text{ Hz}$ was applied to the LMG. Since the equivalent electrical resistance of the LMG changes rapidly even during one discharge pulse, and even more so from pulse to pulse [24], the amplitude values of the voltage on the LMG and the current in it, as well as the total duration of the modes of the discharge pulses changed noticeably, and we can only talk about approximate average values of these parameters. For aluminum LMG, they were 220 V, 180 A and 100 μs , respectively.

The pieces of 999 silver were irregularly shaped. They were bitten off with wire cutter from a sheet 3 mm thick so that the size of the sides was from 3 to 7 mm. Their surface was pre-treated by spark erosion. The height of their layer in DC No. 2 with vertical silver electrodes was 6 mm, the width was 120 mm, and the distance between the electrodes was 60 mm. There was no water flow in this series of experiments. The frequency of forced vibration activation of the LMG in this case was $\approx 40 \text{ Hz}$. The average values of duration of discharge pulses were 30 μs , the voltage amplitude of the pulses was 130 V, and the current was 120 A.

In the absence of complex expensive specialized and not very common optical equipment, such as a monochromator (for example, MDR-2), a photoelectronic multiplier (for example, FEU-106), a high-speed analog-to-digital converter, etc. [25], optical studies were carried out using an ordinary household web camera (WCam in Fig. 1) with mediocre characteristics (matrix 640 by 480 pixels). The images of streamer-leader and spark channel projections obtained with its help were saved on a PC, and then analyzed using the specialized ToupView program of the ToupTek Company [26], which is freely available and designed for working with digital optical cameras of microscopes and telescopes. The program has a wide functionality and, which is important for our research, allows to enlarge the image up to 1600 %, approximate the image of objects with a number of geometric shapes, the parameters of which can be adjusted, as well as measure and calculate their indicators such as area, perimeter, length of axes, etc. [27]. At the time of writing this article, the latest version of the ToupView program 4.11.19728 dated 22.10.2021 has an option to construct ellipses by three points, which is very

convenient and allows to quickly and fairly accurately approximate image elements. The program automatically measures the length of their axes, based on which the values of the volumes of the corresponding ellipsoids of rotation were then calculated, which were used to approximate the areas with colored radiation and spark channels of white color.

Spectral analysis of streamer-leader and spark channels between aluminum granules in water.

A photography of the plasma channels between the surfaces of aluminum granules immersed in distilled water in DC No. 1 in the dark (to increase image contrast) is presented in Fig. 2.

As you can see, the vast majority of channels have a white core and a colored halo, in this case, blue-violet. One of the qualitative criteria for distinguishing spark channels from streamers and leaders is the continuous spectrum of their white radiation. This kind of radiation spectrum is caused by high temperature (about 10,000 K) and pressure (about 100 MPa) in spark channels in such processes, as researchers write about [6].

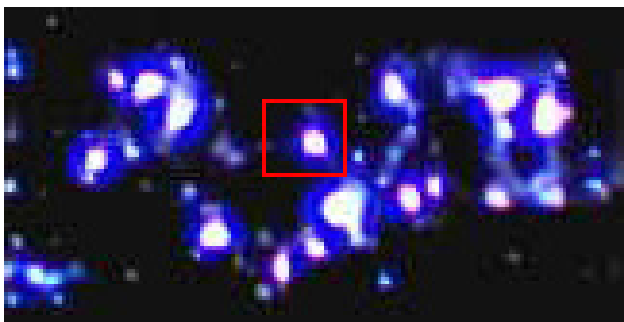


Fig. 2. Plasma channels in the layer of aluminum granules

The temperature of the streamer-leader channels and their pressure are orders of magnitude lower. The main part of their radiation is caused by transitions of electrons in excited atoms to lower orbitals, which causes a linear color spectrum. This makes it possible to carry out a spectral analysis of the chemical composition of excited atoms in and near such channels and to make assumptions about chemical reactions that can occur in such conditions.

The emergence of a halo with colored radiation can occur according to three main mechanisms. According to the first one, the source of excitation of electrons of atoms of the vapor-gas or liquid phase of substances that surround the spark cores can be the ultraviolet radiation of the spark core. That is, the emission of the halo is secondary, induced as a result of higher-energy radiation of the core [28]. The following facts testify in favor of this mechanism: 1) almost all halos have a spark core and almost all spark cores are surrounded by colored halos; 2) in the vast majority of cases, the halos are located around the spark cores quasi-uniformly from all sides.

According to the second mechanism, the excitation of atoms around the spark core is caused by their collisions with fast electrons and ions in streamer-leader avalanches [29]. Even in a homogeneous gas dielectric, streamers and leaders spread along a zigzag path, which ensures the smallest drop in electric voltage across it [30]. This way of expansion of electronic and ion avalanches of

streamers and leaders is all the more characteristic of heterogeneous dielectrics. As long as one of the leaders does not evolve into a spark channel, they can repeatedly appear, change their position in space, and even disappear in a relatively long time (on the order of 30 ms), during which a slow digital household camera captures a frame. Due to the migration and branching of streamers and leaders, the volume they permeate during this time is usually greater than the volume of the spark channel. This mechanism is supported by the fact that there is no strict spatial symmetry of the halo relative to the core.

According to the third mechanism, ionization of atoms occurs in an electric field of high intensity, especially near eroded metal particles in the working liquid, which has a relatively low specific electrical conductivity, and microprotrusions on the surface of metal granules, as occurs in dielectrics near inclusions with higher electrical conductivity [31, 32]. Obviously, this ionization mechanism is primary and can lead to the occurrence of the two discussed above. In our opinion, to one degree or another, all three mechanisms of ionization or excitation of atoms are present in the considered conditions. That is, the second mechanism should occur in a statistically significant number of cases. Then it is logical to assume that the volume and intensity of emission of colored halos are related to the energy that is released specifically in the streamer and leader channels and the distribution of their volumes can be correlated with the size distribution of the nanosized fraction of eroded metal particles.

If the first mechanism of excitation or ionization of atoms prevails, then the volume and intensity of radiation of each colored halo will be proportional to the energy released in the corresponding spark cores. In this case, the ratio of the halo volumes to the core volumes will not change significantly, and only the analysis of the distribution of the spark core volumes will be sufficient to predict the size distribution of the eroded metal particles.

Spectrometric analysis of halo radiation requires appropriate equipment capable of accurately determining the length of all radiation wavelengths, which allows atoms to be identified by their spectral lines, comparing them with reference data [33]. But an approximate spectral analysis based on the resulting shade of the brightest emission lines can also provide certain information about the predominant atoms in the excited state and allows predicting possible chemical reactions involving them.

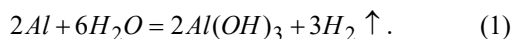
In the general case, excited electrons of neutral atoms of aluminum (Al) and its ions (Al^+ and Al^{2+}), as well as molecules of its compounds, for example, oxide (Al_2O_3), returning to their orbitals, emit photons in the ultraviolet and visible ranges of the spectrum of electromagnetic waves [33–38]. According to the analysis of scientific publications, the highest intensity of radiation (in order of its decrease in various experiments) is observed for waves of the following lengths: 396.15, 394.4, 308.21, 309.27 and 309.28 nm for Al (in the literature on spectrometry it is designated as $Al I$) [34–37], 466.4, 499.8, 484.5, 487, 489, 467, 470, 472, 456, and 474 nm for Al^+ (accepted to be denote as $Al II$) [34], 510.5, 508, 512.5, 514.5, 516, 519 and 520.5 nm for

Al_2O_3 (accepted to be denote as *AlO I*) [35] and 451.3 nm for Al^{2+} (accepted to be denote as *Al III*) and 358.7 nm for Al^+ [38].

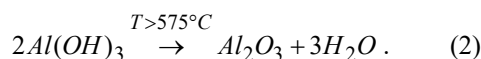
The objects of emission spectra research and the conditions of the experiments described in the literature were as follows. In [34] – plasma formations that arose in a hydrogen atmosphere with pressure of 13.3 kPa due to the irradiation of an aluminum plate with neodymium laser with power density of 300 GW/cm². In [35] – the flame of combustion in the air flow of aluminum particles with average diameter of 4.2 μm. Plasma channels in strong aqueous electrolytes H_3BO_3 and $Na_2B_4O_7$ [36] and KOH and Na_2SiO_3 [37] in the processes of plasma-electrolytic anodization of aluminum. In [38] – plasma formations that arose as a result of the bombardment of aluminum target with Xe^+ ions with energies of the order of 10 ke·V in a vacuum of 10⁻⁶ Pa.

Nanoporous Al_2O_3 is capable of luminescent radiation in a relatively wide range of wavelengths, approximately from 380 to 500 nm (at the half-maximum level) [40, 41] due to the action of near-ultraviolet radiation [39] or electric currents of plasma channels in it. This radiation can last several hundreds of microseconds longer than the action of its exciting factor [42].

Electromagnetic radiation with wavelength of approximately 390 to 440 nm is interpreted by the human eye as violet, from 440 to 480 as blue, and from 480 to 510 as cyan [43]. That is, the vast majority of the relaxation radiation of Al , Al^+ , Al^{2+} and Al_2O_3 forms light of blue and violet colors and only a small part of it forms blue light, or belongs to the ultraviolet range. Therefore, the halos in Fig. 2 have a blue-violet color, which indirectly indicates the presence of aluminum ions, its atoms and their compounds, primarily oxide and hydroxide, in the plasma channels and in their immediate vicinity. Given the fact that the processes take place in water, the most likely chemical reactions of aluminum hydroxide formation take place [13]:



This is possible only under conditions of destruction of the surface oxide film, for example, under the influence of electrical energy. After the formation of aluminum hydroxide according to reaction (1), the processes of further dehydration of a small part of it under the influence of high temperature of plasma channels are possible, according to the reaction:



Since in the described processes aluminum hydroxide and oxide are formed according to reactions (1) and (2), ultraviolet radiation from spark cores is also present, the luminescent radiation described in [39–41] also occurs.

Development of a method of optometric analysis of the ratio of the volumes of colored halos and spark channels in LMG. The shape of most plasma channels between two spherical metal electrodes, in the absence of other inhomogeneities, of all known stereometric bodies, the geometric location of surface points of which is easily described analytically, most resembles an ellipsoid

[20, 44]. Due to the uniformity of conditions in homogeneous environments, this ellipsoid can be an ellipsoid of rotation around an axis that coincides with the resulting direction of current flow from one electrode to another. Although in LMG the plasma channels between their surfaces do not always have the correct and symmetrical shape, with a certain approximation they can also be represented by ellipsoids of rotation of equivalent volume.

Since the dimensions of the DC are small enough to significantly attenuate the radiation of plasma channels in the working liquid, and the walls of DC No. 1 made of organic glass and DC No. 2 made of polyethylene are thin enough and transparent in the visible part of the spectrum of electromagnetic radiation, it can be assumed that the photographs show full projections both a bright spark core and a dim colored halo around it, presumably caused by streamer-leader channels. To determine the volume of the ellipsoid of rotation V_r , it is enough to know only the length of its semi-axis of rotation o_r and the length of one of the other two equal semi-axes o_p : $V_r = 4\pi o_r o_p^2 / 3$. This is very appropriate, since in order to determine the length of all three semi-axes of an ellipsoid, in general, it is necessary to have at least two pictures of it synchronized in time in different (preferably orthogonal) projections, which is impossible to do with one camera without additional mirrors or prisms.

The projection of an ellipsoid onto any plane is an ellipse. The camera is located so that the directions of the resulting currents in all vertical layers of granules are in planes parallel to the plane of its image. This creates the conditions for the majority of images of plasma channels to display the axes of ellipsoids of equivalent volume in their natural size without distortion. Since the direction of current flow in the local elements of the LMG is determined not by the shortest geometric distance between the DC's electrodes, but by the smallest electrical resistance of these elements, there is a possibility that it may be located at an angle to the picture plane.

Let us denote the angles between the plane of the image and the semi-axis of rotation of such an ellipsoid α , and between this plane and one of its other two semi-axes β . Then the length of the projections of these semi-axes on the image plane will be $o'_r = o_r \cdot \cos \alpha$ and $o'_p = o_p \cdot \cos \beta$, respectively. The volume of the spark core approximated by such an ellipsoid calculated from the projections of the semi-axes will be $V_s = 4\pi \cdot o'_r \cdot o'^2_{ps} / (3 \cdot \cos \alpha \cdot \cos^2 \beta)$. If the directions of the corresponding axes of the equivalent ellipsoids of the spark core o_{rs} and o_{ps} and the color halo o_{rl} and o_{pl} coincide, then its volume will be $V_L = 4\pi (o'_{rl} \cdot o'^2_{pl} - o'_{rs} \cdot o'^2_{ps}) / (3 \cdot \cos \alpha \cdot \cos^2 \beta)$. The ratio of the volumes of the equivalent ellipsoids of the halo and core in this case will be $V_L / V_s = (o'_{rl} \cdot o'^2_{pl}) / (o'_{rs} \cdot o'^2_{ps}) - 1$. Therefore, if we analyze the ratio of volumes, and not their absolute values, then under the assumptions described above, the angles of inclination of the axes of the ellipsoids of rotation of the equivalent volume to the image plane do not matter. Also in this case, the units of measurement of length (pixels or millimeters) do not matter, and instead of the length of the semi-axes, it is possible to use the length of the axes, since their

coefficients of 0.5 cancel each other, which is convenient for working with the ToupView program, which measures the length of the axes, not the semi-axes of ellipses.

The question of which of the two axes of the elliptic projection is the projection of the axis of rotation of the ellipsoid remains open. If the distance between the electrodes significantly exceeds the size of the irregularities on their surface, then with greater probability, the larger axis is the axis of rotation of the ellipsoid and it is elongated. If the distance between the electrodes is commensurate to the size of the irregularities on their surface, then with a greater probability the smaller axis is the axis of rotation of the ellipsoid and it is flattened. Since the pressure on the granules is lower in the upper part of the LMG, the probability of the appearance of plasma channels increases, the shape of which resembles an elongated ellipsoid of rotation, while in the lower part of the LMG, on the contrary, it is flattened. Therefore, under the described conditions, both options are possible, therefore, one should find appropriate relations for both elongated (index 1) and flattened (index 2) ellipsoids of rotation.

One of the factors that significantly affects the mass and size of eroded metal particles is the energy of individual plasma channels, which is spent on heating, melting, vaporizing, and evacuating the metal from the granule zones that are in direct contact with the plasma channels [13]. In streamer-leader channels, this energy is orders of magnitude lower than in spark channels [20]. Therefore, the mass and size of erosion particles obtained as a result of the action of streamer-leader channels are orders of magnitude smaller than those of particles obtained as a result of the action of spark channels. The volume of channels, their brightness and time of existence are related to the energy released in them. An increase in the volume and brightness of channels leads to an increase the quantity, and in some cases, the size of erosion particles. Therefore, an increase the quantity and size of streamer-leader channels leads to an increase increase the quantity of particles with unit sizes of tens of micrometers. Accordingly, the ratio of the volumes of streamer-leader and spark channels affects the ratio of the quantity of submicron erosion particles to erosion particles of larger sizes.

By reducing the size of spark channels, which have a white emission color, it is possible to reduce the quantity, and in some cases, the size of larger erosion particles. However, it should be remembered that the productivity of the process of obtaining them will also decrease. By increasing the size of colored streamer-leader channels, the quantity of small submicron erosion particles can be increased. An increase in the volume ratio of streamer-leader channels to spark channels contributes to an increase in the share of submicron erosion particles.

The energy of individual plasma channels depends on the voltage $u_1(t)$ applied to them, their electrical

resistance $r_1(u_1(t))$, which also depends on it, and the time of their existence τ_1 and can be calculated by the formula:

$$E_1 = \int_0^{\tau_1} [u_1^2(t)/r_1(u_1(t))] dt. \quad (3)$$

As practice has shown, the voltage of the discharge pulses is the parameter that most affects the size, brightness, and number of spark channels during spark erosion treatment of LMG. Therefore, control of energy (3), brightness and volumes of streamer-leader and spark channels, as well as the ratio of their volumes in these modes occurs, first of all, with the help of the voltage of discharge pulses. Controlling these parameters using the duration of discharge pulses (by changing the capacity of the working capacitor in thyristor generators or the time of the open state of the key in transistor generators) during spark erosion treatment is less effective. In the case of plasma erosion treatment of LMG, the voltage of the discharge pulses is kept as low as possible for the established process and is almost not subject to regulation. Therefore, in this case, a more effective parameter for adjusting the volumes of streamer-leader and spark channels, as well as their ratio, is the duration of discharge pulses.

One of the plasma channels with a size close to the statistical average in Fig. 2 is marked with a red rectangle. This section of the image is shown on a larger scale (800 % in ToupView) in Fig. 3. Approximation of the projection of the spark core in Fig. 3 is represented by a red ellipse and labeled E1. The length of its axes of 6 and 5 pixels (px) is automatically calculated in the ToupView program and presented in Fig. 3. Approximation of the projection of the colored halo in Fig. 3 is represented by a fuchsia ellipse and is labeled E2. The length of its axes is 14 and 12 pixels. Crosses of the corresponding colors in Fig. 3 mark the characteristic points by which the ToupView program built these ellipses.

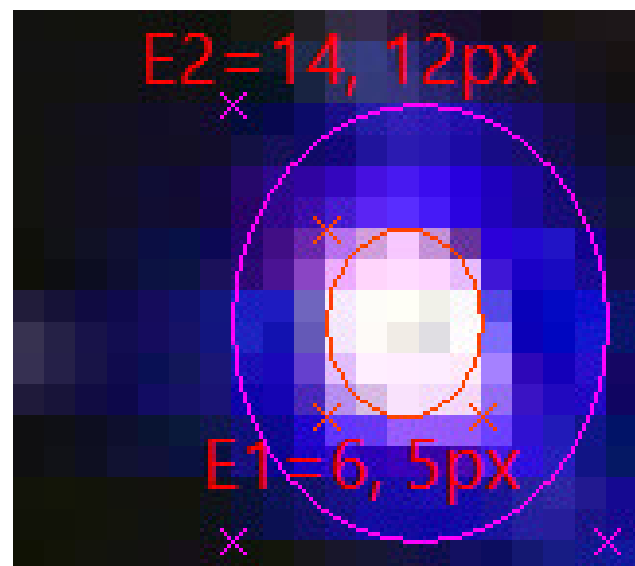


Fig. 3. Plasma channel between aluminum granules

In the hypothesis of elongated ellipsoids, the ratio of the volumes of the halo and core is $V_{L1}/V_{S1} = (14 \cdot 12^2)/(6 \cdot 5^2) - 1 \approx 12.44$, and in the hypothesis

of flattened ellipsoids: $V_{L2}/V_{S2}=(12 \cdot 14^2)/(5 \cdot 6^2)-1 \approx 12.07$. Since, in this particular case, the length of the major and minor axes of each ellipsoid differs slightly, the results obtained in different hypotheses are almost identical. To accurately determine the energy released in the core and halo, it is necessary to know the power density distributions in their volumes, their dependence on time, and the duration of the channels' existence. Such research requires more sophisticated equipment. Here, we can only qualitatively estimate the energy ratio of the colored halo, presumably caused by the streamers, and the spark core, based on the ratio of their volumes and brightness.

A situation is possible when some plasma channels do not have a spark core, but consist entirely of streamer-leader halos, or very bright spark cores have almost no streamer-leader halos. Then it makes sense to determine separately the sums of the volumes of all streamer-leader halos and spark cores presented in the image, and then find their ratio.

The developed method consists in measuring the volumes of colored halos and spark cores of plasma channels in the LMG by images of their projections and the involvement of specialized software and finding their ratios. The obtained information is used for predictions of size distributions of eroded metal particles, including the ratio of their nano- and micro-sized fractions and correction of their properties during the production process by adjusting the voltage and duration of discharge pulses.

Analysis of parameters of color halos and spark channels between silver granules in water. One of the characteristic plasma channels in the LMG of silver on a scale of 250 % is presented in Fig. 4. Unlike the previous picture, this picture was taken in a lit laboratory, because not only the spark core, but also the colored halo in this case were bright enough and did not need darkness to photograph them. As in the experiments with LMG of aluminum, the projection of the bright spark core in Fig. 4 is approximated by a red ellipse with axis lengths of 22 and 17 pixels, which is labeled E1. Approximation of the projection of the colored halo in Fig. 4 is represented by a fuchsia ellipse with axis lengths of 50 and 45 pixels and labeled E2. Crosses of the corresponding colors mark the characteristic points at which the ToupView program built these ellipses.

In the hypothesis of elongated ellipsoids, the ratio of the volumes of the halo and core in this case is $V_{L1}/V_{S1}=(50 \cdot 45^2)/(22 \cdot 17^2)-1 \approx 14.92$, and in the hypothesis of flattened ones: $V_{L2}/V_{S2}=(45 \cdot 50^2)/(17 \cdot 22^2)-1 \approx 12.67$. In this case, the results obtained under different hypotheses differ from each other a little more than in the previous one, since the differences between the lengths of the axes of the ellipsoids are also larger. The greater the ratio of the volume of the colored halo to the volume of the spark core, the greater the probability of obtaining eroded metal particles of smaller sizes, which in the case of silver increases the biocidal activity of hydrosols based on them [15, 16].

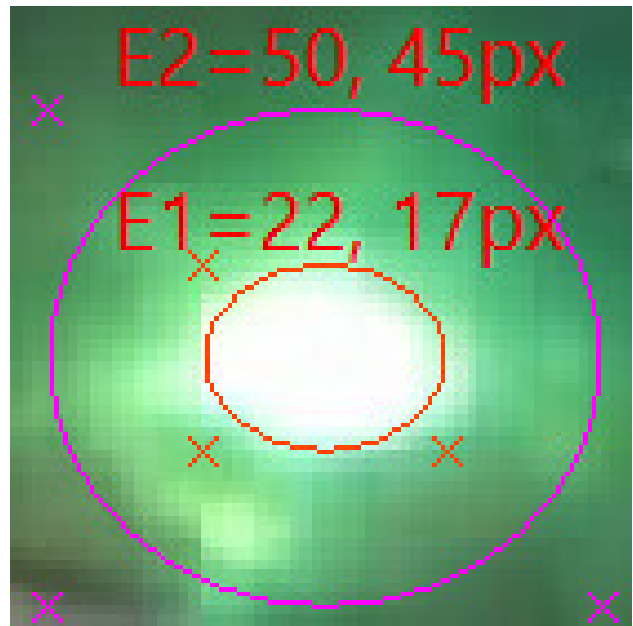
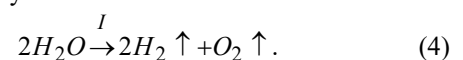


Fig. 4. Plasma channel between silver granules

The halo of the plasma channel between the silver granules is green. Near the white spark core, there is a shade of green mint, and further away from it, an emerald shade, which may be associated with a decrease in the intensity of the white radiation of the core with distance from it. Under the conditions of an underwater spark discharge between Ag granules, the highest radiation intensity of its neutral atoms (accepted to be denote as *Ag I*) is observed at two wavelengths: 546.5 and 520.9 nm (transitions of electrons from the $5d^2D$ levels to the $5p^2P^0$ levels) [45, 46]. The radiation intensity of excited neutral *Ag* atoms is also observed at wavelengths 466.8 and 447.6 nm (transitions from $7s^2S$ to $5p^2P^0$) and at 768.8 and 827.4 nm (transitions from $6s^2S$ to $5p^2P^0$) [45, 46]. There is also a relatively low intensity emission of excited silver ions Ag^+ (denoted *Ag II*) at wavelengths of 540.01 nm (transition from $4d^94f$ to $4d^95d$) and 489.13 nm (transition from $4d^85s^2$ to $4d^95p$) [45].

It is described in [45] that relatively low-intensity radiation with wavelengths of 656.3 nm, which belongs to the first (alpha) transition of the Balmer series in hydrogen atoms (H_α) and 777.42 nm, which belongs to excited neutral oxygen atoms (*O I*) [33]. It is known that molecular oxygen at altitudes from 80 to 150 km under the influence of the solar wind emits a green aurora with wavelength of 557.7 nm [47]. Oxygen molecules are formed on the silver anode as a result of the electrochemical decomposition of water under the action of unipolar discharge pulses [48], since oxygen does not react very actively with silver:



Under the influence of electric currents and radiation of the spark core, electrons in oxygen molecules can move to higher energy levels, and after returning from them – emit photons with the specified wavelength. That is, radiation with wavelength of 557.7 nm can be an indirect indication of the existence or formation of oxygen molecules in plasma channels, for example, as a result of reaction (4).

Electromagnetic radiation with wavelength of approximately 510 to 550 nm is interpreted by the human eye as green, and from 550 to 575 nm as yellow-green [43]. That is, the brightest spectral lines of radiation in the LMG of silver form shades of the resulting green color.

Simplification of the method of spectral estimation of plasma between granules of a number of metals in some working liquids. When the amplitude of the voltage pulses in the aluminum LMG is increased to ≈ 400 V, the character of the plasma channels between them changes somewhat. First, the linear dimensions of the channels increase by 2–5 times. Secondly, the intensity of light and the specific size of the spark core, which now occupies almost the entire volume of the plasma channel, increase significantly. Thirdly, outside the spark core, sometimes in addition to the blue-violet halo, and sometimes instead of it, a halo strip of pale purple or pale pink hue appears. The probability of its occurrence increases slightly in the case of an increase in the speed of the flow of water directed from the bottom up, which contributes to an increase in the average distance between the surfaces of neighboring granules.

The color of this additional halo is similar to the color of the radiation of excited hydrogen atoms both in the composition of the H_2 gas molecule and in the composition of the H_2O molecule of water vapor, which are formed as a result of heating water by plasma channels. This color is determined by the combination of radiation of the most intense lines of the Balmer series in the visible part of the spectrum with wavelengths of $H_\alpha=656.3$ nm red, $H_\beta=486.1$ nm blue, and violet colors: $H_\gamma=434.1$ nm, $H_\delta=410.2$ nm and $H_\epsilon=397.0$ nm. If the intensity of all these lines is equal, the result will be a pale purple hue, and if the intensity of the H_α line predominates, it will be pale pink.

In our experiments on spark erosion treatment of low-alloy steel LMG both in water and in ethanol [49], under the conditions of voltage pulse amplitude values of more than 300 V, a narrow pale yellow halo was observed with the naked eye around the bright spark core of the plasma channels. The increase in its size and light intensity was caused by an increase in the energy of the pulses, the frequency of their repetition, as well as the flow rate of the working liquid and the intensity of air purging of the LMG, the direction of which was from the bottom up, which contributed to an increase in the average distance between the granules.

Spectral studies of the radiation of plasma channels in water between iron granules showed that the most intense emission lines of neutral Fe atoms (denoted $Fe I$) have wavelengths in the range from 560 to 590 nm [46, 50], which corresponds to the yellow color (575–585 nm) and its shades from yellow-green (550–575 nm) to orange (585–620 nm) [43]. The radiation also contains the above-described $H_\alpha=656.3$ nm and $O I=777.1$ nm lines, and a group of low-intensity lines with wavelengths in the range from 490 to 540 nm, which belong to $Fe I$ [45, 50].

In the processes of spark- and plasma-erosion production of copper hydrosols resistant to sedimentation

[15], we observed a narrow, dull strip of halo of malachite-nephrite green color around the spark core of the channel. Spectral studies of the radiation of such channels showed that the highest intensity (in decreasing order) was the emission lines of neutral Cu atoms (denoted $Cu I$) with wavelengths of 521.8, 515.3, 510.5, 465.1, 529.3, and 458.6 nm [51], which corresponds to the short-wavelength region of the green color range (510–550 nm) and the blue color range (480–510 nm) [43]. As in the case of plasma channels in water between the granules of some other metals, there are H_α , H_β , $O I=777.1$ nm lines and lines of low intensity $Cu I$ radiation: 570.0, 578.2, 793.3 and 809.2 nm [51], whose contribution to the color of the total radiation is insignificant.

When we obtained spark-erosion particles of $Ni-Mn-Ga$ alloys with magnetic shape memory [1] and hydrogen-absorbing $Ti-Zr-Ni$ alloys [7] in liquid nitrogen, bright and large halos of plasma channels of the resulting blue-blue in color, and in liquid argon of $Ti-Zr-Ni$ alloys [7] – violet-blue color of lower brightness. In liquid nitrogen, the lines of the ionized nitrogen molecule N_2^+ (denoted $N_2 II$) with wavelengths of 391.4 and 427.8 nm have the highest radiation intensity [52, 53]. In descending order of radiation intensity, the spectral lines of the neutral nitrogen molecule N_2 (denoted $N_2 I$) with wavelengths of 394.3, 575.5, 470.9, 551.6, and 537.3 nm follow [54]. There is also a series of low-intensity spectral lines with wavelengths in the range from 457.4 to 470.9 nm [54], which the human eye interprets as blue [43].

In neutral Ar atoms (denoted $Ar I$), lines with wavelengths of 420.07, 415.86, 427.22, 419.83, 425.94, 430.01, 433.36, 426.63, 404.44, 418.19, 394.9, 416.42, 433.53, 434.52 and 425.12 nm have the highest radiation intensity (in descending order) [55]. The radiation of these lines is interpreted by the human eye as a violet color, the wavelength of which is in the range from 390 to 440 nm [43]. In the radiation of argon ions Ar^+ (denoted $Ar II$), in order of decreasing radiation intensity, there are lines with wavelengths of 459.0, 472.7, 440.1, 501.7, 476.5, 461.0, 488.0, 427, 8, 434.8, 480.6, 454.5 nm, etc. [56], which correspond to violet (390–440 nm), blue (440–480 nm), and cyan (480–510 nm) colors [43]. The results of spectral studies are summarized in Table 1.

The first column presents atoms, ions and molecules of chemical elements that were present in the plasma channels and had spectral lines of radiation of noticeable intensity. Their designations adopted in spectrometry are given in parentheses. The second column shows the wavelengths of the five brightest spectral emission lines of these elements. A more complete list of spectral emission lines of these elements is given above. The third column presents the common name of the shade that most closely matches the color of the resulting radiation in the subjective opinion of the authors, as well as the approximate range of wavelengths of radiation of the main colors of this shade.










An approximate view of the shade of radiation is presented in the fourth column. The shade of the resulting radiation is affected by many factors: the brightness of the spark core of the plasma channels and the distance of the

observation point from it, the degree and frequency dependence of radiation absorption by the working liquid and the material of the walls of the discharge chamber, their reflection of external light, its spectrum and brightness, etc. In addition, the appearance of the shade on the monitor screen is also affected by its settings

(brightness, contrast, gamma correction, color temperature) and the corresponding graphics card settings. Listed in Table 1 examples are correct for the initial values of the video card settings of the Samsung R508 laptop on which they were reproduced: gamma = 1, brightness = 0, contrast = 50.

Table 1

Results of spectral studies of plasma channels halos radiation

Atom, ion, molecule	The wavelength of the brightest lines λ , nm	Name of the resulting shade of radiation	Approximate appearance of the shade	RGB shade code
<i>Al (Al I), Al⁺ (Al II), Al²⁺ (Al III), Al₂O₃ (AlO I)</i>	396,2, 394,4, 484,5, 466,4, 451,3	Blue-violet (390–480 nm)		R=60, G=0, B=255
<i>Ag (Ag I), Ag⁺ (Ag II)</i>	546,5, 520,9, 540,0, 489,1	Emerald (510–550 nm)		R=75, G=170, B=90
		Green mint (510–550 nm)		R=150, G=230, B=140
<i>Cu (Cu I)</i>	521,8, 515,3, 510,5, 465,1, 529,3	Malachite-jade (510–530 nm)		R=30, G=145, B=50
<i>Fe (Fe I), Fe⁺ (Fe II)</i>	558,6, 557,2, 562,4, 576,3, 591,4	Pale yellow (575–585 nm)		R=255, G=255, B=170
<i>H (H I)</i>	656,3, 486,1, 434,1, 410,2, 397,0	Pale purple (397–656 nm)		R=220, G=90, B=255
	656,3	Pale pink (656 nm)		R=255, G=195, B=195
<i>N₂ (N₂ I), N₂⁺ (N₂ II)</i>	391,4, 427,8, 394,3, 575,5, 470,9, 551,6	Blue-cyan (440–510 nm)		R=100, G=150, B=255
<i>Ar (Ar I)</i>	420,1, 415,9, 427,2, 459,0, 472,7, 440,1	Violet-blue (390–480 nm)		R=150, G=120, B=255

To increase the objectivity of the reproduction of shades on different devices, their RGB code is given in the fifth column. Values are obtained using Photoshop's eyedropper tool for the most characteristic areas of colored halos in their digital photographs. If the shades of the halos differed significantly when moving away from the spark cores of the plasma channels, as in the case of *Ag*, or due to a change in the power and conditions in the local plasma channels, as in the case of *H*, then the fourth and fifth columns present the two most characteristic shades and their RGB codes respectively.

Analysis of the shade of the resulting radiation is much simpler than its spectrometric analysis, which requires expensive and complex highly specialized equipment. The proposed analysis is based on the previously obtained results of the spectrometric analysis of the radiation of excited atoms of specific metals and their surrounding working liquids in conditions close to the modes of their spark and plasma erosion processing.

Generalization and conclusions.

1. An optometric method was developed for determining the volumes of colored halos, presumably caused by streamers, and spark cores of plasma channels between metal granules immersed in the working liquid and their ratio, which does not require specialized spectrometric equipment. The obtained values indicate the energies of streamer-leader and spark channels between metal granules and their ratio, which affect the size distribution of erosion particles, including the ratio of their nano- and micro-sized fractions. Their use is expedient when adjusting the modes of spark- and

plasma-erosion electrotechnological processes in order to increase the specific share of erosion particles of the required sizes.

2. In spark erosion technologies, the voltage of the discharge pulses has the greatest influence on the size, brightness and quantity of spark channels, so its use to control these parameters is of primary importance compared to the duration of the discharge pulses. In plasma erosion technologies, the voltage of the discharge pulses is kept as low as possible for the steady-state process and is almost not subject to regulation. Instead, the main adjustment parameter in this case is the duration of discharge pulses.

3. The possibility of simplifying the spectrometric method of analyzing the plasma and its surrounding vapor-gas phase in the LMG based on the analysis of the shade of the resulting radiation, which is based on previously obtained spectrometric data, is substantiated.

4. An analysis of the emission spectra of colored halos of plasma channels in distilled water between *Al*, *Ag*, *Fe* and *Cu* granules and *Ni-Mn-Ga* and *Ti-Zr-Ni* in liquid nitrogen and *Ti-Zr-Ni* in liquid argon is carried out. The shades of the resulting emission of halos in these cases are substantiated and summarized, and their description by RGB codes is provided.

5. Based on the analysis of the emission spectra of colored halos of plasma channels in distilled water, which are caused by an electric current, it was confirmed that the reactions of hydrogen gas formation, and in the case of silver granules, also oxygen as a result of the electrochemical decomposition of water, took place.

During the spark-erosion dispersion of aluminum granules in water, the occurrence of chemical reactions of the formation of its hydroxide, as well as a small part of the oxide under the influence of high temperatures of the spark channels, was indirectly confirmed.

Acknowledgment. The work was carried out with the support of the Ministry of Education and Science of Ukraine (Project DB No. 0121U107443).

Conflict of interest. The authors of the article declare that there is no conflict of interest.

REFERENCES

- Ochin P., Gilchuk A.V., Monastyrsky G.E., Koval Y., Shcherba A.A., Zaharchenko S.N. Martensitic Transformation in Spark Plasma Sintered Compacts of Ni-Mn-Ga Powders Prepared by Spark Erosion Method in Cryogenic Liquids. *Materials Science Forum*, 2013, vol. 738-739, pp. 451-455. doi: <https://doi.org/10.4028/www.scientific.net/MSF.738-739.451>.
- Monastyrsky G. Nanoparticles formation mechanisms through the spark erosion of alloys in cryogenic liquids. *Nanoscale Research Letters*, 2015, vol. 10, no. 1, art. no. 503. doi: <https://doi.org/10.1186/s11671-015-1212-9>.
- Aur S., Egami T., Berkowitz A.E., Walter J.L. Atomic Structure of Amorphous Particles Produced by Spark Erosion. *Physical Review B*, 1982, vol. 26, no. 12, pp. 6355-6361. doi: <https://doi.org/10.1103/PhysRevB.26.6355>.
- Hong J.I., Parker F.T., Solomon V.C., Madras P., Smith D.J., Berkowitz A.E. Fabrication of spherical particles with mixed amorphous/crystalline nanostructured cores and insulating oxide shells. *Journal of Materials Research*, 2008, vol. 23, no. 06, pp. 1758-1763. doi: <https://doi.org/10.1557/JMR.2008.0199>.
- Wang W., Zhu F., Weng J., Xiao J., Lai W. Nanoparticle morphology in a granular Cu-Co alloy with giant magnetoresistance. *Applied Physics Letters*, 1998, vol. 72, no. 9, pp. 1118-1120. doi: <https://doi.org/10.1063/1.120942>.
- Berkowitz A.E., Hansen M.F., Parker F.T., Vecchio K.S., Spada F.E., Lavernia E.J., Rodriguez R. Amorphous soft magnetic particles produced by spark erosion. *Journal of Magnetism and Magnetic Materials*, 2003, vol. 254-255, pp. 1-6. doi: [https://doi.org/10.1016/S0304-8853\(02\)00932-0](https://doi.org/10.1016/S0304-8853(02)00932-0).
- Kolbasov G.Ya., Ustinov A.I., Shcherba A.A., Perekos A.Ye., Danilov M.O., Vyunova N.V., Zakharchenko S.N., Hossbah G. Application of volumetric electric-spark dispersion for the fabrication of Ti-Zr-Ni hydrogen storage alloys. *Journal of Power Sources*, 2005, vol. 150, pp. 276-281. doi: <https://doi.org/10.1016/j.jpowsour.2005.02.025>.
- Jin C.H., Si P.Z., Xiao X.F., Feng H., Wu Q., Ge H.L., Zhong M. Structure and magnetic properties of Cr/Cr₂O₃/CrO₂ microspheres prepared by spark erosion and oxidation under high pressure of oxygen. *Materials Letters*, 2013, vol. 92, pp. 213-215. doi: <https://doi.org/10.1016/j.matlet.2012.10.126>.
- Harrington T., McElfresh C., Vecchio K.S. Spark erosion as a high-throughput method for producing bimodal nanostructured 316L stainless steel powder. *Powder Technology*, 2018, vol. 328, pp. 156-166. doi: <https://doi.org/10.1016/j.powtec.2018.01.012>.
- Berkowitz A.E., Walter J.L. Spark Erosion: A Method for Producing Rapidly Quenched Fine Powders. *Journal of Materials Research*, 1987, no. 2, pp. 277-288. doi: <https://doi.org/10.1557/JMR.1987.0277>.
- Carrey J., Radovsky H.B., Berkowitz A.E. Spark-eroded particles: influence of processing parameters. *Journal of Applied Physics*, 2004, vol. 95, no. 3, pp. 823-829. doi: <https://doi.org/10.1063/1.1635973>.
- Shen B., Inoue A. Fabrication of large-size Fe-based glassy cores with good soft magnetic properties by spark plasma sintering. *Journal of Materials Research*, 2003, vol. 18, no. 9, pp. 2115-2121. doi: <https://doi.org/10.1557/jmr.2003.0297>.
- Shydlovska N.A., Zakharchenko S.M., Zakharchenko M.F., Mazurenko I.L., Kulida M.A. Physical and Technical-economic Aspects of Modern Methods of Water Treatment for Thermal and Nuclear Power Engineering. *Technical Electrodynamics*, 2022, no. 4, pp. 69-77. (Ukr). doi: <https://doi.org/10.15407/techned2022.04.069>.
- Goncharuk V.V., Shcherba A.A., Zakharchenko S.N., Savluk O.S., Potapchenko N.G., Kosinova V.N. Disinfectant action of the volume electrospark discharges in water. *Khimii i tehnologiiia vody*, 1999, vol. 21, no. 3, pp. 328-336. (Rus).
- Shcherba A.A., Zakharchenko S.N., Lopatko K.G., Aftandilyants E.G. Application of volume electric spark dispersion for production steady to sedimentation hydrosols of biological active metals. *Pratsi Instytutu Elektrodynamiky Natsionalnoi Akademii Nauk Ukrainy*, 2009, no. 22, pp. 74-79. (Rus).
- Zakharchenko S.M., Shydlovska N.A., Perekos A.O., Lopatko K.G., Savluk O.S. Features of Obtaining of Plasma-Erosion Nanodispersed Silver Hydrosols and Their Bactericidal and Fungicidal Properties. *Metallofizika i Noveishie Tekhnologii*, 2020, vol. 42, no. 6, pp. 829-851. (Rus). doi: <https://doi.org/10.15407/mfint.42.06.0829>.
- Batsmanova L., Taran N., Konotop Ye., Kalenska S., Novytska N. Use of a Colloidal Solutions of Metal and Metal Oxide-Containing Nanoparticles as Fertilizer for Increasing Soybean Productivity. *Journal of Central European Agriculture*, 2020, vol. 21, no. 2, pp. 311-319. doi: <https://doi.org/10.5513/JCEA01.21.2.2414>.
- Youssef F.S., El-Banna H.A., Elzorba H.Y., Gabal A.M. Application of Some Nanoparticles in the Field of Veterinary Medicine. *International Journal of Veterinary Science and Medicine*, 2019, vol. 7, no. 1, pp. 78-93. doi: <https://doi.org/10.1080/23144599.2019.1691379>.
- Shydlovska N.A., Zakharchenko S.M., Cherkaskyi O.P. Physical Prerequisites of Construction of Mathematical Models of Electric Resistance of Plasma-erosive Loads. *Technical Electrodynamics*, 2017, no. 2, pp. 5-12. (Ukr) doi: <https://doi.org/10.15407/techned2017.02.005>.
- Raizer Yu.P. *Gas Discharge Physics*. Berlin, Springer, 1991. 449 p.
- Lo A., Cessou A., Lacour C., Lecordier B., Boubert P., Xu D., Laux C.O., Vervisch P. Streamer-to-spark transition initiated by a nanosecond overvoltage pulsed discharge in air. *Plasma Sources Science and Technology*, 2017, vol. 26, no. 4, art. no. 045012. doi: <https://doi.org/10.1088/1361-6595/aa5c78>.
- Shcherba A.A., Zakharchenko S.N., Yatsyuk S.A., Kucheryavaya I.N., Lopatko K.G., Aftandilyants E.G. Analysis of the Methods of Increasing the Efficiency of Electric-erosive Coagulation During Cleaning of Aqueous Media. *Technical Electrodynamics. Thematic Issue «Power Electronics and Energy Efficiency»*, 2008, part 2, pp. 120-125. (Rus).
- Shcherba A.A., Zakharchenko S.N., Suprunovskaya N.I., Shevchenko N.I. The influence of repetition rate of discharge pulses on electrical resistance of current-conducting granular layer during its electric-spark treatment. *Technical Electrodynamics*, 2006, no. 2, pp. 10-14.
- Shcherba A.A., Suprunovska N.I., Ivashchenko D.S. Determination of Probabilistic Properties of Electrical Characteristics of Circuits of Electric Discharge Installations Taking into Account their Stochastically Changing Parameters. *Technical Electrodynamics*, 2019, no. 4, pp. 3-11. (Rus). doi: <https://doi.org/10.15407/techned2019.04.003>.

25. Shuaibov O.K., Malinina A.O., Hrytsak R.V., Malinin O.M., Bilak Yu.Yu., Gomoki Z.T., Vatralla M.I. Characteristics and Parameters of Overstressed Nanosecond Discharge Between Copper Electrodes in Argon. *Metallofizika i Noveishie Tekhnologii*, 2021, vol. 43, no. 12. pp. 1683-1706. (Ukr). doi: <https://doi.org/10.15407/mfint.43.12.1683>.
26. Touptek. Download. Available at: <https://www.touptek.com/download> (Accessed 15 March 2023).
27. Touptek. Download. Software Download. Help files for ToupCam camera. Available at: <http://www.touptek.com/download/showdownload.php?lang=en&id=7> (Accessed 15 March 2023).
28. Medvedev N., Zastrau U., Forster E., Gericke D.O., Rethfeld B. Short-Time Electron Dynamics in Aluminum Excited by Femtosecond Extreme Ultraviolet Radiation. *Physical Review Letters*, 2011, vol. 107, art. no. 165003. doi: <https://doi.org/10.1103/PhysRevLett.107.165003>.
29. Kim S.J., Lee Y.S., Cho Ch.H., Choi M.S., Seong I.H., Lee J.J., Kim D.W., You Sh.J. Observation of prior light emission before arcing development in a low-temperature plasma with multiple snapshot analysis. *Scientific Reports*, 2022, no. 12, art. no. 20976. doi: <https://doi.org/10.1038/s41598-022-25550-2>.
30. Baranov M.I. A generalized physical principle of development of plasma channel of a high-voltage pulse spark discharge in a dielectric. *Electrical Engineering & Electromechanics*, 2024, no. 1, pp. 34-42. doi: <https://doi.org/10.20998/2074-272X.2024.1.05>.
31. Shcherba A.A., Shcherba M.A., Peretyatko Ju.V. Electro-Physical Processes of Degradation of Cross-Linked Polyethylene Insulation of Power Cables and Self-Carrying Insulated Wires under Non-Sinusoidal Voltages and Currents. *Technical Electrodynamics*, 2023, no. 1. pp. 3-6. (Ukr). doi: <https://doi.org/10.15407/techned2023.01.03>.
32. Bereka V.O., Bozhko I.V., Kondratenko I.P. Influence of Parameters of Water Movement at its Treatments on Energy Efficiency Pulse Barrier Discharge. *Technical Electrodynamics*, 2022, no. 3, pp. 62-68. (Ukr). doi: <https://doi.org/10.15407/techned2022.03.062>.
33. Zaidel' A.N., Prokof'ev V.K., Raikii S.M., Slavnyi V.A., Shreider E.Ya. *Tables of Spectral Lines*. New York, Springer, 1970. 782 p. doi: <https://doi.org/10.1007/978-1-4757-1601-6>.
34. Parigger C.G., Hornkohl J.O., Nemes L. Measurements of aluminum and hydrogen microplasma. *Applied Optics*, 2007, vol. 46, no. 19, pp. 4026-4031. doi: <https://doi.org/10.1364/AO.46.004026>.
35. Soo M., Goroshin S., Glumac N., Kumashiro K., Vickery J., Frost D.L., Bergthorson J.M. Emission and Laser Absorption Spectroscopy of Flat Flames in Aluminum Suspensions. *Combustion and Flame*, 2017, vol. 180, pp. 230-238. doi: <https://doi.org/10.1016/j.combustflame.2017.03.006>.
36. Sarvan M., Radić-Perić J., Kasalica B., Belča I., Stojadinović S., Perić M. Investigation of Long-duration Plasma Electrolytic Oxidation of Aluminum by Means of Optical Spectroscopy. *Surface & Coatings Technology*, 2014, vol. 254, pp. 270-276. doi: <https://doi.org/10.1016/j.surfcoat.2014.06.029>.
37. Liu R., Wu J., Xue W., Qu Ya., Yang Ch., Wang B., Wu X. Discharge Behaviors During Plasma Electrolytic Oxidation on Aluminum Alloy. *Materials Chemistry and Physics*, 2014, vol. 148, no. 1-2, pp. 284-292. doi: <https://doi.org/10.1016/j.matchemphys.2014.07.045>.
38. Qayyum A., Akhtar M.N., Riffat T. Light Emission from Sputtered Aluminum Atoms and Ions Produced by Ion Bombardment. *Radiation Physics and Chemistry*, 2005, vol. 72, no. 6, pp. 663-667. doi: <https://doi.org/10.1016/j.radphyschem.2004.05.048>.
39. Stojadinovic S., Vasilic R., Petkovic M., Nedic Z., Kasalica B., Belca I., Zekovic Lj. Luminescence properties of oxide films formed by anodization of aluminum in 12-tungstophosphoric acid. *Electrochimica Acta*, 2010, vol. 55, no. 12, pp. 3857-3863. doi: <https://doi.org/10.1016/j.electacta.2010.02.011>.
40. Staninski K., Piskula Z., Kaczmarek M. Photo- and electroluminescence properties of lanthanide tungstatedoped porous anodic aluminum oxide. *Optical Materials*, 2017, vol. 64, pp. 142-146. doi: <https://doi.org/10.1016/j.optmat.2016.12.003>.
41. Stepniowski W.J., Norek M., Michalska-Domanska M., Bombalska A., Nowak-Stepniowska A., Kwasny M., Bojar Z. Fabrication of Anodic Aluminum Oxide with Incorporated Chromate Ions. *Applied Surface Science*, 2012, vol. 259, pp. 324-330. doi: <https://doi.org/10.1016/j.apsusc.2012.07.043>.
42. Shcherba A.A., Shtompel I.V. Analysis electrical parameters and dynamics of spark discharges in a layer of current-conducting granules. *Stabilizatsiia parametrov elektricheskoi energii*, 1991, pp. 65-74. (Rus).
43. Abcibc.com. Light wavelengths. Available at: <http://abcibc.com/photo-reference-tables.php?art=19> (Accessed 15 March 2023). (Rus).
44. Nijdam S., Teunissen J., Ebert U. The physics of streamer discharge phenomena. *Plasma Sources Science and Technology*, 2020, vol. 29, no. 10, art. no. 103001. doi: <https://doi.org/10.1088/1361-6595/abaa05>.
45. Ninyovskij V., Murmantsev A., Veklich A., Boretskij V. Plasma spectroscopy of electric spark discharge between silver granules immersed in water. *Energetika*, 2022, vol. 68, no. 1, pp. 107-114. doi: <https://doi.org/10.6001/energetika.v68i1.4862>.
46. Veklich A., Tmenova T., Zazimko O., Trach V., Lopatko K., Titova L., Boretskij V., Aftandilyants Ye., Lopatko S., Rogovskiy I. Regulation of Biological Processes with Complexions of Metals Produced by Underwater Spark Discharge. *Nanooptics and Photonics, Nanochemistry and Nanobiotechnology and Their Applications: Selected Proceedings of the 7th International Conference Nanotechnology and Nanomaterials (NANO2019)*, pp. 283-306. doi: https://doi.org/10.1007/978-3-030-52268-1_23.
47. Aurora. Available at: <https://en.wikipedia.org/wiki/Aurora> (Accessed 15 March 2023).
48. Shydlovska N.A., Zakharchenko S.M., Cherkassky O.P. The Analysis of Electromagnetic Processes in Output Circuit of the Generator of Discharge Pulses with Non-linear Model of Plasma-erosive Load at Change Their Parameters in Wide Ranges. *Technical Electrodynamics*, 2016, no. 1, pp. 87-95. (Rus). doi: <https://doi.org/10.15407/techned2016.01.087>.
49. Zakharchenko S.M., Perekos A.O., Shydlovska N.A., Ustinov A.I., Boytsov O.F., Voynash V.Z. Electrospark Dispersion of Metal Materials. I. Influence of Velocity of Flow of Operating Fluid on Dispersion of Powders. *Metallofizika i Noveishie Tekhnologii*, 2018, vol. 40, no. 3, pp. 339-357 (Rus). doi: <https://doi.org/10.15407/mfint.40.03.0339>.
50. Murmantsev A., Veklich A., Boretskij V. Optical emission spectroscopy of plasma of electric spark discharge between metal granules in liquid. *Applied Nanoscience*, 2023, vol. 13, no. 7, pp. 5231-5237. doi: <https://doi.org/10.1007/s13204-022-02744-8>.
51. Tmenova T.A., Veklich A.N., Boretskij V.F., Cressault Y., Valensi F., Lopatko K.G., Aftandilyants Y.G. Optical Emission Spectroscopy of Plasma Underwater Electric Spark Discharges Between Metal Granules. *Problems of Atomic Science and Technology*, 2017, vol. 107, no. 1, pp. 132-135.
52. Li S.-Y., Li S.-C., Sui L.-Z., Jiang Y.-F., Chen A.-M., Jin M.-X. Contribution of nitrogen atoms and ions to the

luminescence emission during femtosecond filamentation in air. *Physical Review A*, 2016, vol. 93, no. 1, art. no. 013405. doi: <https://doi.org/10.1103/PhysRevA.93.013405>.

53. Lianzhu Z., Shuxia Z., Xiulan M. Characterization of Nitrogen Glow Discharge Plasma via Optical Emission Spectrum Simulation. *Plasma Science and Technology*, 2008, vol. 10, no. 4, pp. 455-462. doi: <https://doi.org/10.1088/1009-0630/10/4/11>.

54. Wang Z., Cohen S.A., Ruzic D.N., Goeckner M.J. Nitrogen atom energy distributions in a hollow-cathode planar sputtering magnetron. *Physical Review E*, 2000, vol. 61, no. 2, pp. 1904-1911. doi: <https://doi.org/10.1103/PhysRevE.61.1904>.

55. Bogaerts A., Gijbels R., Vlcek J. Modeling of glow discharge optical emission spectrometry: Calculation of the argon atomic optical emission spectrum. *Spectrochimica Acta Part B: Atomic Spectroscopy*, 1998, vol. 53, no. 11, pp. 1517-1526. doi: [https://doi.org/10.1016/S0584-8547\(98\)00139-6](https://doi.org/10.1016/S0584-8547(98)00139-6).

56. Saloman E.B. Energy Levels and Observed Spectral Lines of Ionized Argon, Ar II through Ar XVIII. *Journal of Physical and Chemical Reference Data*, 2010, vol. 39, no. 3, art. no. 033101. doi: <https://doi.org/10.1063/1.3337661>.

How to cite this article:

Shydlovska N.A., Zakharchenko S.M., Zakharchenko M.F., Kulida M.A., Zakusilo S.A. Spectral and optic-metric methods of monitoring parameters of plasma channels caused by discharge currents between metals granules in working liquids. *Electrical Engineering & Electromechanics*, 2024, no. 6, pp. 72-83. doi: <https://doi.org/10.20998/2074-272X.2024.6.10>

Received 18.03.2024

Accepted 31.05.2024

Published 21.10.2024

N.A. Shydlovska¹, Corresponding Member of NAS of Ukraine, Doctor of Technical Science, Chief Research Scientist, S.M. Zakharchenko¹, Doctor of Technical Science, Leading Research Scientist,

M.F. Zakharchenko², Candidate of Chemical Sciences,

M.A. Kulida³, Candidate of Veterinary Sciences,

S.A. Zakusilo¹, Postgraduate Student,

¹Institute of Electrodynamics

of the National Academy of Sciences of Ukraine,

56, Prospect Beresteiskiyi, Kyiv, 03057, Ukraine,

e-mail: snzakhar@ukr.net (Corresponding Author)

²V.I. Vernadsky Institute of General and Inorganic Chemistry

of the National Academy of Sciences of Ukraine,

32/34, Prospect Palladina, Kyiv, 03142, Ukraine.

³National University of Life and Environmental Sciences of

Ukraine,

16, Vystavkova Str., Kyiv, 03041, Ukraine.